Vibrational Conical Intersections as a Mechanism of Ultrafast Vibrational Relaxation

Peter Hamm[1] and Gerhard Stock[2]

[1]*Physikalisch-Chemisches Institut, Universität Zürich, Winterthurerstrasse 190, CH-8057 Zürich, Switzerland*
[2]*Biomolecular Dynamics, Institute of Physics, Albert Ludwigs University, 79104 Freiburg, Germany*

(Received 9 June 2012; published 23 October 2012)

Presenting true crossings of adiabatic potential energy surfaces, conical intersections are a paradigm of ultrafast and efficient electronic relaxation dynamics. The same mechanism is shown to apply also for vibrational conical intersections, which may occur when two high-frequency modes (such as OH stretch vibrations) are coupled to low-frequency modes (such as hydrogen bonding modes). By derivation of a model Hamiltonian and its parametrization for a concrete example, malonaldehyde, the conditions that such conical intersections occur are identified and the consequences for the vibrational dynamics and spectra are demonstrated.

DOI: 10.1103/PhysRevLett.109.173201 PACS numbers: 34.50.Ez

Ever since their theoretical prediction by von Neumann and Wigner in 1929 [1], conical intersections (CIs) have become a paradigm of ultrafast photochemical or photophysical processes [2–4]. CIs are true crossings of two Born-Oppenheimer (or adiabatic) potential energy surfaces [PESs, see Fig. 1(a)], which may lead to extremely fast and efficient transfer of population between the two electronic states. At the crossing surface the nonadiabatic interaction diverges, which results in a complete breakdown of the Born-Oppenheimer approximation. Hence a perturbative description of the dynamics in terms of electronic relaxation rates is not sufficient, and time-resolved pump-probe experiments on CIs may reveal complex spectral features [5–7].

The situation appears to be quite different in the case of *vibrational* relaxation dynamics in the electronic ground state. Here relaxation dynamics and transient spectra are often well described within a perturbative approach by simply assuming a $1/T_1$ relaxation rate [8–11]. However, there are cases where—quite similar to the vibronic case—this approach seems to break down [12]. In particular, vibrational bands that are associated with strong hydrogen bonding are typically very broad (many 100 cm^{-1}), strongly redshifted and contain a pronounced substructure due to strong anharmonic couplings to other modes [13,14]. The nonlinear pump-probe response of these infrared transitions, in turn, decays on an ultrafast (a few 100 fs) time scale and may exhibit complex oscillatory features [15,16]. Also, liquid water [17] and ice [18] are found to show an extremely fast initial signal that has been attributed to population decay. If excess protons are added to water (i.e., acid solutions), a continuum band covering almost the whole mid-IR range from 1000–3000 cm^{-1} is observed [19].

In this Letter, we propose that vibrational CIs may represent a possible mechanism for ultrafast vibrational relaxation dynamics. To introduce the general idea, we note that an adiabatic perspective is also sometimes taken for vibrational states, e.g., when a high-frequency mode (such as a OH stretch vibration) is coupled to a low-frequency mode (such as a hydrogen bond mode, whose frequency is about 10 times lower) [14,20–23]. Solving the Schrödinger equation for the high frequency mode with the low frequency coordinate introduced parametrically, this leads to potential energy surfaces for the vibrational states of the high-frequency modes as a function of the low-frequency coordinates. However, to the best of our knowledge, the concept of a CI has not been used in the context of vibrational adiabatic states. A Jahn-Teller type of coupling has been discussed in the context of vibrational transitions [24,25], which in fact leads to a CI dictated by symmetry, but that connection has not been made. In this Letter, we derive the conditions that such an intersection occurs, present quantum-dynamical model calculations to show the consequences for the vibrational dynamics and spectra, and demonstrate via *ab initio* calculations that low-lying vibrational CIs indeed exist in concrete molecular systems.

The minimum ingredients needed to construct a vibrational CI include two high-frequency (HF) modes, q_1 and

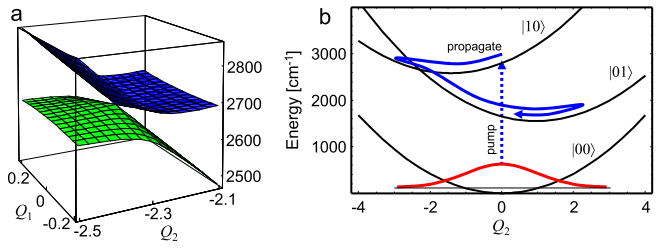

FIG. 1 (color online). (a) CI between two adiabatic PESs along a coupling mode Q_1 and a tuning mode Q_2, revealing a funnel-like shape of the PESs at the intersection point. (b) Cuts of the vibrational PESs along Q_2 for $Q_1 = 0$, using the parameters given in Table I. The ground state wave function is excited by an ultrashort laser pulse and subsequently propagates as indicated by the arrow.

q_2, as well as two low-frequency (LF) modes, Q_1 and Q_2. We require at least two HF modes to assure that two vibrational states may become degenerate, either by symmetry via a Jahn-Teller type of coupling [24,25] or accidentally (which is the case we will focus on). On the other hand, at least two LF modes are needed because the hypersurface of a CI is (N-2)-dimensional (N being the number of LF modes). The Hamiltonian of the model can be written as $H = H_0 + H_{\text{anh}}$ with

$$H_0 = \sum_n \frac{\omega_n}{2}(p_n^2 + q_n^2) + \sum_j \frac{\Omega_j}{2}(P_j^2 + Q_j^2),$$
$$H_{\text{anh}} = \sum_{n,m,j} f_{nm,j} q_n q_m Q_j, \tag{1}$$

where n, m, $j = 1, 2$ and $\hbar = 1$. H_0 represents the harmonic part of the Hamiltonian, expressed in terms of vibrational frequencies (ω_n, Ω_j) and dimensionless normal mode coordinates (q_n, Q_j) and momenta (p_n, P_j). The anharmonic interaction H_{anh} is obtained via a Taylor expansion. While all cubic as well as higher-order expansion coefficients will have an effect on the PESs in detail, we will see that a minimal model of a vibrational CI requires only two types of cubic expansion coefficients, the coupling parameter $f_{12,1}$ and the tuning parameters $f_{nn,2}$.

We expand the total vibrational wave function as

$$|\Phi(Q)\rangle = \sum_k \Psi_k(Q)|k\rangle, \tag{2}$$

that is, the HF modes are represented by the zero-order harmonic basis states $|k\rangle = |00\rangle, |10\rangle, |01\rangle, \ldots$, where $|ij\rangle$ denote the number of quanta in modes q_1 and q_2, respectively, and the LF modes are represented by the wave functions $\Psi_k(Q)$ with $Q = \{Q_1, Q_2\}$. Restricting ourselves to the first three states $|k\rangle$, we represent Hamiltonian (1) as 3×3 matrix $\mathcal{H} = \{\langle k|H|k'\rangle\}$, giving

$$\mathcal{H} = h_0 \mathbf{1} + \begin{pmatrix} \kappa_{00} Q_2 & 0 & 0 \\ 0 & \omega_1 + \kappa_{10} Q_2 & \lambda Q_1 \\ 0 & \lambda Q_1 & \omega_2 + \kappa_{01} Q_2 \end{pmatrix}, \tag{3}$$

with $h_0 = \sum_j \frac{\Omega_j}{2}(P_j^2 + Q_j^2)$ and $\mathbf{1}$ being the unit matrix. The diagonal elements of $\mathcal{H}$ consist of the LF harmonic Hamiltonian, the excitation energy ω_n of the HF modes (the zero-point energy is neglected), and the couplings $\kappa_k Q_2$. To obtain the latter from Eq. (1), we assumed that mode Q_2 couples only diagonal elements (i.e., $f_{nm,2} = 0$ for $n \neq m$), which yields

$$\kappa_k = \sum_n f_{nn,2} \langle k|q_n^2|k\rangle. \tag{4}$$

Since this LF mode modulates the vibrational excitation energy of the HF modes [via $\omega_k^{\text{dia}}(Q_2) = \omega_k + \kappa_k Q_2$], we henceforth refer to Q_2 as "tuning coordinate." Note that κ_{00} may be nonzero, describing the deformation of the potential energy surface with respect to the LF coordinates upon trying to minimize the zero-point energy of the HF modes.

Similarly, Q_1 is assumed to couple exclusively off-diagonally (i.e., $f_{nn,1} = 0$), yielding

$$\lambda = f_{12,1}\langle 10|q_1 q_2|01\rangle = f_{21,1}\langle 01|q_2 q_1|10\rangle. \tag{5}$$

This way, the LF mode Q_1 couples the HF modes q_1 and q_2, with the amount of the mixing depending on Q_1 (i.e., the mixing vanishes for $Q_1 = 0$). Hence we will refer to Q_1 as "coupling coordinate." Generalizations of the model, e.g., to include several tuning coordinates (via $\kappa_k Q_2 \rightarrow \sum_j \kappa_k^{(j)} Q_j$), several coupling coordinates, or more than two HF modes, are straightforward.

Although Eq. (3) was derived above to account for the coupling of HF and LF vibrational modes, it is formally entirely equivalent to a *vibronic-coupling* Hamiltonian, consisting of the ground and two excited *electronic* states that interact via vibrational tuning and coupling coordinates [26]. In particular, Eq. (3) gives rise to a CI of the adiabatic PESs of the problem. To see this, we note that Hamiltonian (3) is given in the so-called diabatic representation, where the kinetic energy $\sum_j \Omega_j/2 P_j^2$ is diagonal and the potential energy is given as a matrix $\mathcal{V} = \{V_{k,k'}\}$. Diagonalization of this potential-energy matrix yields the adiabatic PESs of the two excited states

$$W_{\mp}(Q_1, Q_2) = \bar{V}(Q_1, Q_2) \mp \sqrt{\Delta V^2(Q_2) + V_C^2(Q_1)}, \tag{6}$$

where $\bar{V} = (V_{10,10} + V_{01,01})/2$, $\Delta V = (V_{10,10} - V_{01,01})/2$ and $V_C = V_{10,01} = V_{01,10}$. A CI of these two surfaces arises for $W_- = W_+$, that is, if $\Delta V(Q_2) = 0$ and $V_C(Q_1) = 0$. For a single tuning and a single coupling coordinate (i.e., $N = 2$), we obtain a crossing point, in general we have an N-2-dimensional intersection surface. We note in passing that the derivation of Hamiltonian (3) from Eq. (1) is the converse of the so-called mapping approach [27] used in the classical description of nonadiabatic quantum dynamics, where an N-state system is mapped onto N harmonic oscillators.

To illustrate the theory developed above, we adopt a set of representative parameters for model Hamiltonian (3) given in Table I. Figure 1(b) presents the resulting diabatic PESs $V_{k,k}(Q_1, Q_2)$ along Q_2 for $Q_1 = 0$ for the three considered states $|k\rangle = |00\rangle, |10\rangle$ and $|01\rangle$, and Fig. 1(a) focuses on the CI. We now assume that all (HF and LF) vibrational modes of the system are initially in their ground state and that at time $t = 0$ an ultrashort infrared laser pulse excites the $|00\rangle \rightarrow |10\rangle$ transition of the HF mode q_1. In direct analogy to the vibronic case, this corresponds to a vertical Franck Condon-type excitation of the LF vibrational wave packet into the excited state $|10\rangle$. Being a nonstationary state, the wave packet will evolve on the coupled PESs of states $|10\rangle$ and $|01\rangle$, thus giving rise to

TABLE I. Parameters (in cm^{-1}) of the model Hamiltonian (3) employed in Figs. 1 and 2. We set $\kappa_{00}^{(j)} = 0$ (which results in a shift of the origin of Q_2) and chose the parameters of the three-mode model such that the diagonal potential elements $V_{k,k}$ along $Q_2 = Q_3$ are identical to the ones of the two-mode model shown in Fig. 1(a).

Model	ω_1	ω_2	Ω_1	λ	Ω_2	$\kappa_{10}^{(2)}$	$\kappa_{01}^{(2)}$	Ω_3	$\kappa_{10}^{(3)}$	$\kappa_{01}^{(3)}$
2 modes	2800	1650	290	200	210	300	−200	...	...	...
3 modes	2800	1650	290	200	230	232	−155	190	192	−128

nonadiabatic wave packet dynamics along the LF coordinates Q_1 and Q_2.

A key quantity in the discussion of nonadiabatic dynamics is the time-dependent population probability of the initially prepared "diabatic" state $|10\rangle$, $P_{10}(t)$, as well as the population $P_{\mathrm{ad}}(t)$ of the corresponding "adiabatic" state defined via Eq. (6) [26]. Propagating the system in time using standard methods [26], the dotted lines in Fig. 2(a) show the evolution of $P_{10}(t)$ and $P_{\mathrm{ad}}(t)$ for a system with two LH modes Q_1 and Q_2. For the chosen parameters, the CI (2665 cm^{-1}) lies below the vertical Franck Condon energy (2800 cm^{-1}); hence, the wave packet reaches the CI within half an oscillation period of Q_2 and there decays into state $|01\rangle$. Subsequently, $P_{10}(t)$ and $P_{\mathrm{ad}}(t)$ are seen to exhibit prominent recurrences, which reflects the finite level density of the two-mode model. Increasing the level density by including a second tuning mode damps the recurrences significantly [solid lines in Fig. 2(a)], quite similar to findings for vibronic CIs [26].

Moreover, Fig. 2(b) shows a three-mode case where the energy of the CI was increased to 3244 cm^{-1} by assuming $\approx 30\%$ smaller tuning parameters. As a consequence, the CI is energetically higher than the initial wave packet, which results in a clearly slower relaxation of the initially excited state. Following essentially an exponential decay, in the case of a high-lying CI the notion of a constant relaxation rate $1/T_1$ seems to become meaningful. We wish to stress, however, that these findings cannot be understood on a simple perturbative level, where, e.g., the tuning term $q_1^2 Q_2 \propto (\hat{b}_1 + \hat{b}_1^\dagger)^2(\hat{B}_2 + \hat{B}_2^\dagger)$, that couples a doubly excited state of q_1 with a singly excited state of Q_2, would be considered to be an extremely inefficient channel for relaxation (as $\omega_1 \gg \Omega_2$). It is rather the (higher-order) interplay of tuning and coupling modes that leads to the ultrafast relaxation process of a CI.

It is interesting to study how the strong vibrational relaxation dynamics is reflected in the time- and frequency-resolved infrared spectra of the system. To calculate these spectra, we employ a nonperturbative approach [28] using resonant ≈ 25 fs Gaussian-shaped pump and probe pulses and assume that all of the oscillator strength sits in mode q_1, such that the laser pulses excite and probe exclusively state $|10\rangle$. To allow for excited state absorption, we furthermore augment Hamiltonian (3) by the doubly excited states $|20\rangle$, $|11\rangle$ and $|02\rangle$, the first of which is lowered by 200 cm^{-1} from its harmonic value to obtain the usual redshift of the 1–2 excited state absorption. Figure 3 shows the resulting transient infrared spectra for the three-mode model. For the sake of interpretation, the total signal (a) is decomposed into the bleach and the stimulated emission contributions (b) and the excited state absorption (c). While the strong negative signal of the bleach band around $\omega_1 = 2800$ cm^{-1} hardly evolves in time, the stimulated emission signal as well as the excited state signal shift to the red extremely rapidly, before they flatten and lose intensity [see feature labeled with (*) in Figs. 3(b) and 3(c)]. This strong redshift is the hallmark of a CI [5,26], as it directly reflects the ultrafast nonadiabatic $|10\rangle \rightarrow |01\rangle$ transition and subsequent wave packet motion on coupled PESs [Fig. 1(b)]. The overall pump-probe response of the simple three-mode model is qualitatively

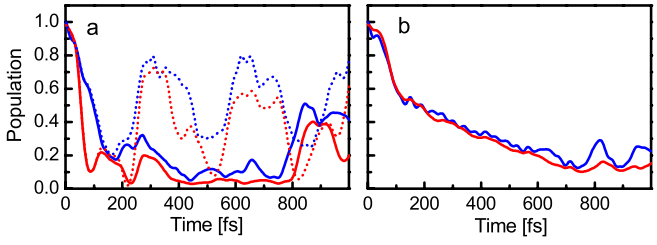

FIG. 2 (color online). Time evolution of the population probability of the initially prepared "diabatic" state $|10\rangle$ [blue (dark grey)] and the corresponding adiabatic population [red (light grey)], following a vertical $|00\rangle \rightarrow |10\rangle$ transition [Fig. 1(b)]. The dotted lines show the results for the two-mode model, solid lines those for the three-mode model (Table I). In panel (b) all tuning parameters of the three-mode model were reduced by 30%.

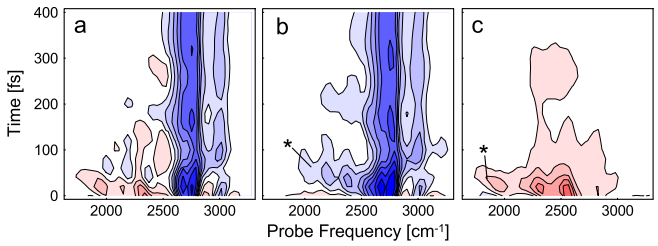

FIG. 3 (color online). Simulated pump-probe spectrum for the three-mode model defined in Table. I. (a) Complete signal, (b) bleach and stimulated emission contribution and (c) excited state absorption. Signals of positive and negative sign are colored in red and blue, respectively. The features labeled with (*) are discussed in the text.

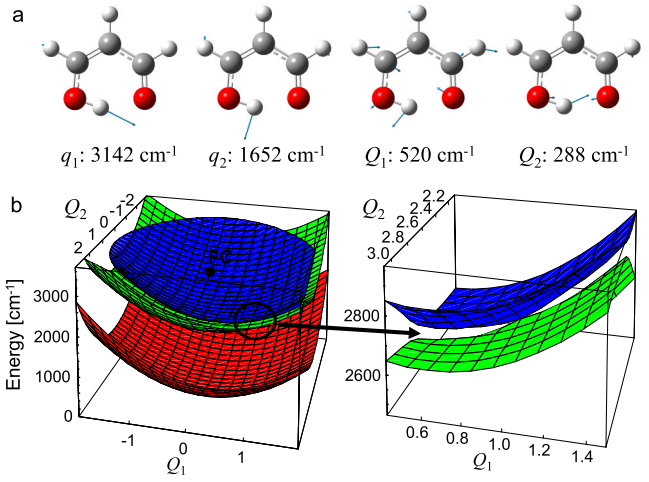

FIG. 4 (color online). Malonaldehyde: (a) Normal modes of interest with their harmonic frequencies. (b) Adiabatic PESs as a function of the LF modes Q_1 and Q_2. The dot marks the Franck Condon (FC) region. The right panel focuses on the CI between the two first excited states.

quite similar to the experimental response of strong intramolecular hydrogen bonds [15,16].

It is obvious from the above discussion that vibrational CIs do exist, since there is no reason to assume that all tuning and coupling constants are zero in the anharmonic PES [Eq. (1)] of a given molecule. However, it remains to be shown that there are concrete molecular systems which exhibit large enough couplings to yield a CI below the initially excited Franck-Condon region. Only then will the intersection provide mechanisms for ultrafast population relaxation. As a proof of principle, we consider malonaldehyde which is a prototype molecule with a medium strong intramolecular hydrogen bond [Fig. 4(a)]. Its tunnel-splitting and intramolecular hydrogen-bond transfer has been studied extensively [14,29–32], while we concentrate here on the dynamics within one of the potential energy wells. We treated the molecule on the MP2/6-311 ++ $g(2df, 2pd)$ quantum-chemical level of theory, using the Gaussian program package [33]. As HF modes, we consider the OH stretch and bend vibrations with harmonic frequencies of 3142 cm^{-1} and 1652 cm^{-1}, respectively. As LF modes, we consider the hydrogen bond vibration (288 cm^{-1}) and the second highest in-plane backbone vibration at 520 cm^{-1} [Fig. 4(a)]. With the "anharmonic" keyword, Gaussian [33] calculates the cubic and quartic expansion coefficients of the PESs, which can be directly used in Hamiltonian (1). In contrast to the idealized model above, the two LF modes act both as tuning *and* coupling modes at the same time. The largest and therefore most important coupling is the tuning parameter of the OH stretch with respect to the hydrogen bond vibration with $f_{11,2} = -246$ cm^{-1}. This large tuning factor reflects the common notion that a OH stretch vibration redshifts upon hydrogen bonding by an amount that is a direct measure of the strength of the hydrogen bond (i.e., essentially of the O $\cdots$ O distance). The tuning parameter of the other mode, $f_{11,1} = -60$ cm^{-1}, is significantly smaller. Both modes have nonzero coupling constants, $f_{12,1} = -75$ cm^{-1} and $f_{12,2} = -80$ cm^{-1}.

Figure 4(b) shows the resulting adiabatic PESs of malonaldehyde as a function of the two LF coordinates. In contrast to the idealized model in Eq. (3), here the complete cubic and quartic potential was used in order to realistically describe the molecule-specific details of the PESs. A CI is found at an energy of 2663 cm^{-1}, which is 146 cm^{-1} below the vertical Franck Condon energy at 2809 cm^{-1}, while the bottom of the $|10\rangle$ surface lies at 2583 cm^{-1}. These values agree roughly with those of the model in Fig. 1; hence, an initially excited wave packet will propagate energetically downhill and relax through the CI in a qualitatively similar way as in Fig. 2.

In conclusion, we have introduced the concept of vibrational CIs. Similar to what was found for their well-known vibronic counterparts, is has been shown that these intersections lead to ultrafast vibrational relaxation dynamics and complex transient infrared spectra. Employing *ab initio* calculations, we have demonstrated that a low-lying vibrational CI of the OH stretch and bend modes may indeed exist for strong intramolecular hydrogen bonds. Only a few LF modes are expected to couple strongly to the HF modes; hence, vibrational energy is selectively funneled into these modes, and could potentially cause reactions such as hydrogen bond breaking [20,34] or proton transfer [21,23]. While full-dimensional wave packet calculations of the ultrafast vibrational relaxation dynamics of various strongly hydrogen-bonded systems are available [14,35,36], the concept of a vibrational CI may add an intuitive physical understanding of these processes. Furthermore, an understanding of vibrational CIs may lead to more accurate approximate algorithms (such as surface hopping [37]) to describe nuclear dynamics.

Future investigations will include the study of intermolecular dynamics, such as that of water in its clustered, liquid or solid form [10,17,18,36]. In direct analogy to the discussion above, the interaction of the OH stretch vibrations among each other and with the hydrogen bonding network is expected to give rise to *intermolecular* vibrational CIs [38], which may help to explain the so-far little understood multidimensional infrared spectra of these systems.

The work has been supported in part by the Swiss National Science Foundation (SNF) through the NCCR MUST.

[1] J. von Neumann and E. Wigner, Phys. Z. **30**, 467 (1929).
[2] *Conical Intersections: Theory, Computation and Experiment*, edited by W. Domcke, D. R. Yarkony, and H. Köppel (World Scientific, Singapore, 2011).

[3] M. A. Robb, M. Garavelli, M. Olivucci, and F. Bernardi, Rev. Comput. Chem. **15**, 87 (2000).
[4] B. Levine and T. Martinez, Annu. Rev. Phys. Chem. **58**, 613 (2007).
[5] G. Stock and W. Domcke, J. Phys. Chem. **97**, 12 466 (1993).
[6] Q. Wang, R. W. Schoenlein, L. A. Peteanu, R. A. Mathies, and C. V. Shank, Science **266**, 422 (1994).
[7] V. Blanchet, M. Z. Zgierski, T. Seideman, and A. Stolow, Nature (London) **401**, 52 (1999).
[8] A. Laubereau and W. Kaiser, Rev. Mod. Phys. **50**, 607 (1978).
[9] J. C. Owrutsky, D. Raftery, and R. M. Hochstrasser, Annu. Rev. Phys. Chem. **45**, 519 (1994).
[10] H. J. Bakker and J. L. Skinner, Chem. Rev. **110**, 1498 (2010).
[11] H. Fujisaki, Y. Zhang, and J. E. Straub, Adv. Chem. Phys. **145**, 1 (2011).
[12] M. Gruebele and P. G. Wolynes, Acc. Chem. Res. **37**, 261 (2004).
[13] O. Henri-Rousseau and P. Blaise, Adv. Chem. Phys. **103**, 1 (1998).
[14] K. Giese, M. Petkovic, H. Naundorf, and O. Kühn, Phys. Rep. **430**, 211 (2006).
[15] J. Stenger, D. Madsen, J. Dreyer, E. T. J. Nibbering, P. Hamm, and T. Elsaesser, J. Phys. Chem. A **105**, 2929 (2001).
[16] D. Madsen, J. Stenger, J. Dreyer, P. Hamm, E. J. Nibbering, and T. Elsaesser, Bull. Chem. Soc. Jpn. **75**, 909 (2002).
[17] M. L. Cowan, B. D. Bruner, N. Huse, J. R. Dwyer, B. Chugh, E. T. J. Nibbering, T. Elsaesser, and R. J. D. Miller, Nature (London) **434**, 199 (2005).
[18] F. Perakis and P. Hamm, Phys. Chem. Chem. Phys. **14**, 6243 (2012).
[19] S. Roberts, P. Petersen, K. Ramasesha, A. Tokmakoff, I. Ufimtsev, and T. Martinez, Proc. Natl. Acad. Sci. U.S.A. **106**, 15 154 (2009).
[20] A. Staib and J. T. Hynes, Chem. Phys. Lett. **204**, 197 (1993).
[21] A. Staib, D. Borgis, and J. T. Hynes, J. Chem. Phys. **102**, 2487 (1995).
[22] G. L. Barnes, S. M. Squires, and E. L. Sibert, J. Phys. Chem. B **112**, 595 (2008).
[23] G. Hanna and E. Geva, J. Phys. Chem. B **115**, 5191 (2011).
[24] T. Oka, J. Chem. Phys. **47**, 5410 (1967).
[25] D. Y. Vorobyev, C.-H. Kuo, D. G. Kuroda, J. N. Scott, J. M. Vanderkooi, and R. M. Hochstrasser, J. Phys. Chem. B **114**, 2944 (2010).
[26] W. Domcke and G. Stock, Adv. Chem. Phys. **100**, 1 (1997).
[27] G. Stock and M. Thoss, Adv. Chem. Phys. **131**, 243 (2005).
[28] L. Seidner, G. Stock, and W. Domcke, J. Chem. Phys. **103**, 3998 (1995).
[29] T. Chiavassa, P. Roubin, L. Pizzala, P. Verlaque, A. Allouche, and F. Marinelli, J. Phys. Chem. **96**, 10 659 (1992).
[30] T. Hayashi and S. Mukamel, J. Phys. Chem. A **107**, 9113 (2003).
[31] T. Hammer and U. Manthe, J. Chem. Phys. **134**, 224305 (2011).
[32] M. Schröder, F. Gatti, and H.-D. Meyer, J. Chem. Phys. **134**, 234307 (2011).
[33] M. J. Frisch *et al.*, *Gaussian 09 Revision A.1* (Gaussian Inc., Wallingford CT, 2009).
[34] T. Steinel, J. B. Asbury, J. Zheng, and M. D. Fayer, J. Phys. Chem. A **108**, 10 957 (2004).
[35] *Multidimensional Quantum Dynamics* edited by H. D. Meyer, F. Gatti, and G. A. Worth (Willey-VCH, Weinheim, 2009).
[36] O. Vendrell, F. Gatti, and H.-D. Meyer, J. Chem. Phys. **127**, 184303 (2007).
[37] J. Tully and R. K. Preston, J. Chem. Phys. **55**, 562 (1971).
[38] S. Wüster, A. Eisfeld, and J. M. Rost, Phys. Rev. Lett. **106**, 153002 (2011).